Planet-Detection Simulations for Several Possible TESS Extended Missions

Luke Bouma, et al.

November 2, 2016

PRM comments in red annotations 11/11/2016

Executive Summary

The Transiting Exoplanet Survey Satellite (*TESS*) will perform a two-year, nearly all-sky survey for transiting exoplanets. There do not appear to be any fundamental obstacles to continuing science operations for at least several years following the Primary Mission. Any Extended Mission will likely need to be organized while the Primary Mission is occupying most of the *TESS* team's attention. The purpose of this white paper is to provide a head start to those who are planning and proposing for an Extended Mission.

Many factors other than prospects for planet detection will likely influence the choice of an Extended Mission. We have created an accompanying Wiki document[1] that can be edited by named members of the community to raise and discuss those broad issues.

This report is focused narrowly on planet detection. Using Monte Carlo simulations, we try to anticipate the quantities and types of planets that would be detected during several plausible scenarios for a one-year Extended Mission following the two-year Primary Mission. Our main focus is on strategies for scanning the sky. For simplicity we do not compare different choices either for the cadence of photometric measurements or for the target stars to be selected, although different choices might prove to be advantageous and should be studied in future work.

Throughout this report we consider six different scenarios for Year 3 of the *TESS* mission, illustrated in Figure 1:

1. `hemi`, which re-observes one of the ecliptic hemispheres in essentially the same manner as in the Primary Mission (i.e., neglecting the zone within 6° of the ecliptic);
2. `hemi+ecl`, which re-observes one of the ecliptic hemispheres, but this time covering the entire hemisphere at the expense of the continuous-viewing zone near the pole;
3. `pole`, which focuses on one of the two ecliptic poles;
4. `ecl_long`, which has a series of pointings with the long axis of the 24° × 96° field-of-view along the ecliptic (in combination with some fields near the ecliptic pole, when the Earth or Moon would prevent effective observations of the ecliptic);
5. `ecl_short`, which has a series of pointings with the short axis of the field-of-view along the ecliptic (again in combination with some fields near the ecliptic pole);
6. `allsky`, which covers nearly the entire sky with 14-day pointings (as opposed to the 28-day pointings of the Primary Mission), by alternating between northern and southern hemispheres.

[1] `https://spacebook.mit.edu/display/TESS/Extended+Missions`. Contact `luke@astro.princeton.edu`, copying `imeister@mit.edu`, for an account with editing rights. The page can be read by anyone.

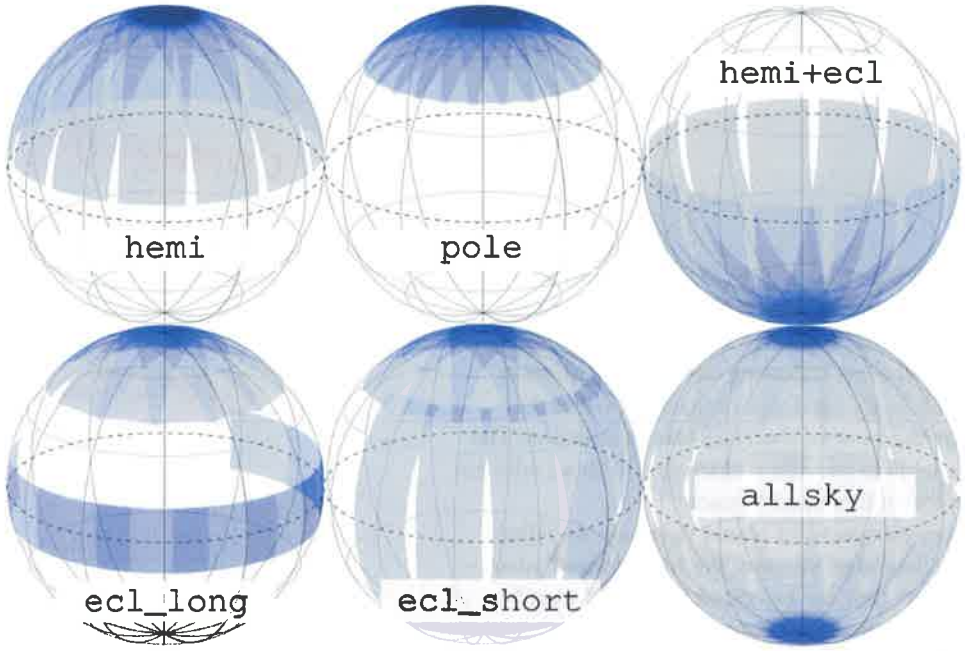

Figure 1: Six proposed pointing strategies for a *TESS* Extended Mission, visualized in ecliptic coordinates. Note that none of these scenarios spend the entire year observing the ecliptic; we concluded that such a plan would be inadvisable because of interruptions by the Earth and Moon (see Fig. 9).

We numerically compute the results based on the methodology of Sullivan et al. [2015], after bug fixes and enhancements by Luke Bouma in consultation with Josh Winn. Additional inputs were provided by Jacobi Kosiarek and Peter McCullough.

Some of the most important findings are:

1. The overall quantity of detected planets* does not depend strongly on the sky-scanning schedule. Among the six scenarios considered here, the number of newly-detected planets with radii less than $4R_\oplus$ is the same to within about 30%.
2. The number of newly-detected sub-Neptune radius planets in Year 3 is approximately the same as the number detected in either Year 1 or Year 2. Thus, we do not expect a sharp fall-off in the planet discovery rate in Year 3. This is because the Primary Mission will leave behind many short-period transiting planets with bright host stars, with a signal-to-noise ratio just below the threshold for detection. These planets can be detected by collecting more data in Year 3.
3. Regarding newly detected sub-Neptunes, the `allsky`, `pole`, and `hemi+ecl` strategies offer the greatest number (1300-1400, as compared to the 1250 during each year of the Primary Mission).
4. Regarding planets with orbital periods >20 days, the `allsky`, `pole`, and `hemi` strategies would discover twice as many such planets as will be discovered in each year of the Primary Mission. This would help to overcome one of the main limitations of the Primary Mission: the strong bias toward shorter orbital periods.
5. Regarding new planets with very bright host stars ($I_c < 10$), the `allsky`, `hemi+ecl`, and `ecl_short` strategies offer the greatest num-

* use a ~~the~~ footnote and cite Eqn on p. 11 as definition of a "detected planet."

← A lot of these are simply changing $N_{tra} = 1$ to $N_{tra} = 2$.

bers (~190, about the same as are found in each year of the Primary Mission; see Table 2).

6. Regarding planets with near-terrestrial insolation ($0.2 < S/S_{\oplus} < 2$), all the strategies considered here offer similar numbers (about 120, as compared to 105 in each year of the Primary Mission).

7. Apart from detecting new planets, a potentially important function of an Extended Mission would be to improve our ability to predict the times of future transits and occultations of *TESS*-detected planets. With data from the Primary Mission alone, the uncertainty in ~~transit ephemerides~~ will inhibit follow-up observations after only a few years, as the transit ephemerides become stale. planetary orbital periods

The rest of this report is organized as follows. Sec. 1 discusses how we selected and compared different pointing strategies, as well as how we modeled *TESS*'s observations and planet detections. Sec. 1.7 gives a list of the most important assumptions we made for the simulations. Sec. 2 compares the ~~simulated populations~~ of newly-detected planets, for the 6 different scenarios under consideration. Sec. 3.1 discusses some considerations and implications for future years of the Extended Mission, beyond the one-year scenarios that were simulated in detail. Sec. 3.2 discusses the critical issue of the uncertainty in transit ephemerides. Sec. 3.3 discusses the reliability and limitations of our methodology. Sec. 4 concludes and recommends avenues for further study.

characteristics

Contents

1 *Approach*

1.1 *Constraints on possible pointing strategies*

When considering possible schedules for telescope pointings, the main constraint is that the cameras must be directed approximately opposite the Sun. Specifically, the center of the combined fields-of-view is ideally pointed within 15° of the antisolar direction, and no more than 30° away. This is necessary for the sunshade and spacecraft to block solar photons. It also enables the solar panels (which are free to rotate about the $+Y$ axis in Fig. 2) to collect sunlight. Given the spacecraft's orbit [Gangestad et al., 2013], this means that *TESS* should advance ∼28° east in ecliptic longitude every lunar month, as it does during the Primary Mission. Focusing on a fixed field for say, 3 spacecraft orbits (≈42 days), would be in tension with this requirement. In practice, another technical restriction is whether the Earth or Moon passes through *TESS*'s camera fields during a proposed pointing (see Sec. 1.6).

In addition, the spacecraft has finite fuel reserves for necessary maneuvers. These are expected to last at least 10 years [G. Ricker, priv. comm.]. We consequently do not consider this as a constraint on the three-year time horizon that is the focus of this study.

1.2 *Our proposed pointing strategies*

For simplicity we chose to study one-year plans for an Extended Mission, i.e., plans for Year 3 of the *TESS* mission. (Later in this report we remark on some possible implications of our study for additional

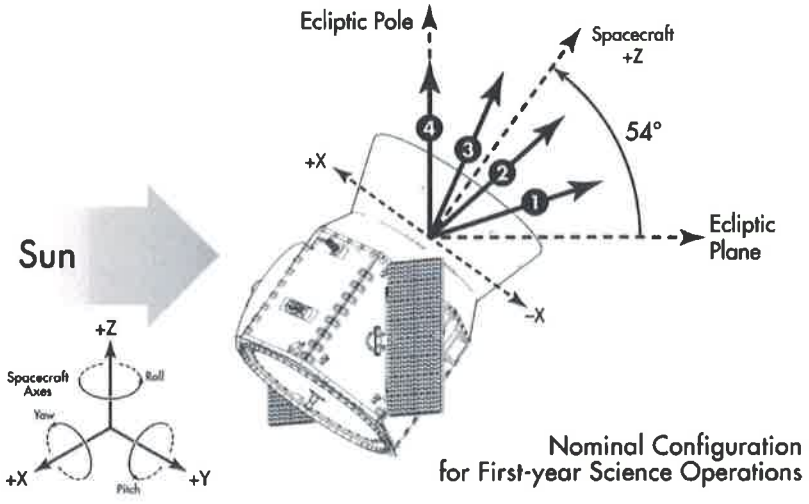

Figure 2: The spacecraft must point so that incident sunlight is collected by the solar panels, and not the cameras. *TESS*'s solar panels pitch about the $+Y$ axis. (Adapted from Orbital ATK design document)

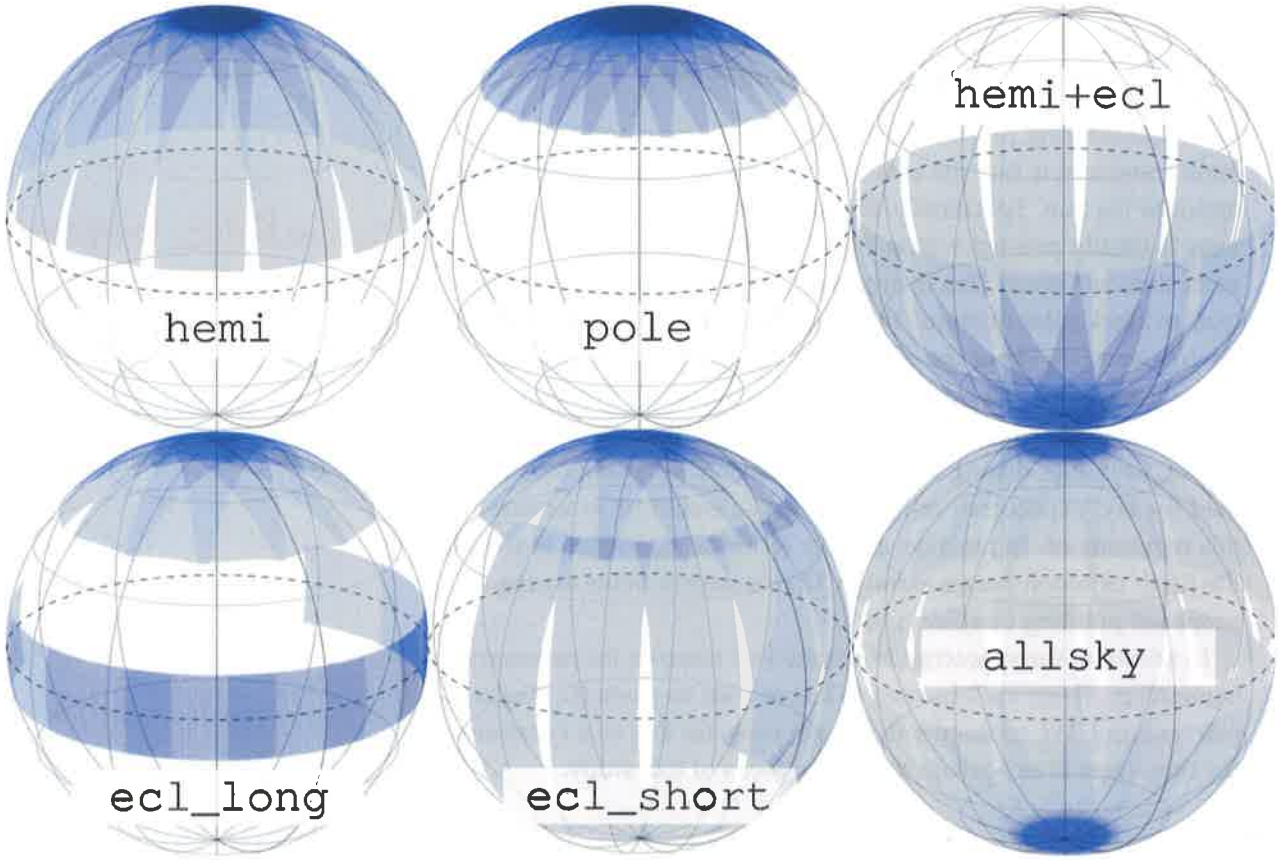

Figure 3: Proposed pointing strategies for a *TESS* Extended Mission, visualized in ecliptic coordinates. `hemi`, `pole`, `hemi+ecl`, `ecl_long`, `ecl_short`, and `allsky`. Note for `ecl_long` and `ecl_short` that Earth and moon crossings likely make an entire year looking at the ecliptic impractical (see Fig. 9).

years of an Extended Mission.) Given the constraints outlined in Sec. 1.1, we selected the following options for detailed study:

Option 1. `hemi`: Repeat observations of one of the two ecliptic hemispheres in a manner similar to the Primary Mission, arbitrarily chosen to be the northern ecliptic hemisphere for concreteness. In this scenario we could take the opportunity to shift the longitudes of all sectors by an amount that would enable *TESS* to cover the gaps that were left during the Primary Mission (the "slits" in the sky coverage between ecliptic latitudes of 6–30°). However for simplicity, we opted to observe the same longitudes as in the Primary Mission. *Justification:* similar motivation as the Primary Mission. Nice long time baseline at the North Ecliptic Pole, and broad sky coverage. Also remeasures transit times (and ~~sharpens~~ substantially improves ephemerides) of previously detected *TESS* planets over most of the entire hemisphere.

Option 2. `pole`: Focus on one of the ecliptic poles, arbitrarily chosen to be the north ecliptic pole for concreteness. Note that the geom-

etry of *TESS*'s lens hood still suppresses incoming sunlight in this scenario. *Justification:* maximizes the average duration of observations per star; intuitively we expected this to provide greatest sensitivity to long-period planets.

Option 3. `hemi+ecl`: Repeat observations of one of the two ecliptic hemispheres, but in this case shifting all fields 12° toward the ecliptic, such that the combined fields-of-view reach all the way from 6° below the ecliptic to the ecliptic pole. *Justification:* trades the long continuous viewing zone near the pole for greater sky coverage, and in particular, coverage of the ecliptic zone which was missed in the Primary Mission. We chose to simulate the southern ecliptic hemisphere, since the northern version of this plan would suffer more from Earth and Moon interference (cf. Table 1 in Sec. 1.6).

Option 4. `ecl_long`: Survey the ecliptic with 7 sectors (14 orbits) in which the long axis of the fields-of-view are oriented along the ecliptic. For the other 6 sectors, during the interval when ecliptic observations would be interrupted by Earth and Moon crossings, we focus on one of the ecliptic poles. *Justification:* covers the ecliptic, which was not surveyed at all in the Primary Mission. Offers opportunities for follow-up of K2 discoveries. Minimizes Earth-moon interference.

Option 5. `ecl_short`: Survey the ecliptic and also cover a large fraction of the rest of the ecliptic hemisphere. For 7 sectors we observe the ecliptic but with the *short* axis oriented along the ecliptic, and the long axis reaching up to higher latitudes. The remaining 6 sectors are focused on the ecliptic pole, as in `ecl_long`. *Justification:* similar to `ecl_long`, but with more overlap between this year and the Primary Mission to allow for improved transit ephemerides and better ability to follow-up on previous discoveries. Also covers more sky than `ecl_long`, which could improve the quantity of planet detections from full frame images.

Option 6. `allsky`: Cover both northern and southern ecliptic hemispheres in a single year, by alternating between the hemispheres every 13.7 days. *Justification:* rapid coverage of the entire sky, allows follow-up of almost all previously detected *TESS* objects and refined ephemerides.

Although these 6 scenarios seemed like reasonable choices for further study and direct comparison, there are many other possibilities that may be of interest that were not studied in detail, in order to keep the scope of this report manageable. Among these other possibilities that were considered but not studied are

* Fig 25 suggest 10^{-9} suppression at $\theta = 90°$, and that's 23 mags so the Sun ($V = -26$) would be like Venus ($V \sim -3$) spread uniformly (more or less) across the detectors. Maybe this OK but I wonder. Is there a source you can cite?

backwards? Table 1 gives 2 for Year 3 selected and 4+3=7 for Year 3 omitted.

- The `pole` strategy applied to the south ecliptic pole rather than the north (we do not expect major differences).
- The `hemi` strategy applied to the southern ecliptic hemipshere rather than the northern (we do not expect major differences). Similarly, the `hemi` strategy, but rotated about the ecliptic polar axis by 12° in longitude.
- The north/south inversion of `hemi+ecl`, which is more strongly affected by Earth and Moon crossings (see Sec. 1.6).
- A full year spent observing the ecliptic. Such a plan would similarly suffer from Earth and Moon crossings for a substantial fraction of the year. We show the outage as a function of time in Fig. 9. Solar system objects (planets, asteroids) could also be an annoyance, but we do not model their effects.
- Alternate between northern and southern ecliptic poles every 13.7 days. This would be similar to `allsky` but would focus on the poles rather than the entire sky. It would sacrifice sky coverage (and ability to refresh ephemerides over the whole sky) in return for longer-duration observations for a typical star.
- Hybrid strategies that change from month to month. For instance, in the `hemi` scenario, during a month when the Earth or Moon crosses through the field of a camera pointed close to the ecliptic, we could tilt all the cameras away from the ecliptic as in the `pole` scenario.

1.3 *Metrics by which we compare pointing strategies*

We assess Extended Missions based on the risks and opportunities they present, as well as through their performance on select technical and science-based criteria. These criteria are organized following an approach originally outlined by Kepner and Tregoe [1965]. Summarizing them in list form:

Technical musts: Cameras anti-sun? Solar panels collecting sunlight?

Technical wants: Duration of each sector < 28 days? Earth or Moon crossings? Zodiacal background? Scattered sunlight off lens hood?

These read as bad things, not wants (?)

Metrics in exoplanet science:

- number of newly detected planets (from 2-minute cadence fixed-aperture target stars, known colloquially as 'postage stamps', as well as 30-minute full frame images – both independently and combined);

- number of new long-period planets (which may be detected through long period coverage, or by follow-up on single-transit events);
- number of new habitable-zone planets;
- number of new planets with "characterizable" atmospheres;
- number of newly detected planets with bright host stars;
- number of stars with transiting planets detected in the Primary Mission for which the Extended Mission reveals an additional transiting planet (usually long-period companions to short-period planets);
- ability to improve transit ephemerides for previously detected transiting planets;
- ability to observe more transits over a longer baseline to enable searches for transit-timing variations.

These metrics were chosen for their apparent importance as well as our ability to quantify them with simulations. Of course there are other considerations that may be very important but are more difficult to quantify:

- Prospects for altering target allocation weights between: white dwarfs, known planet-hosts, candidate planet-hosts, circumbinary & circumprimary planets, open clusters, evolved stars (notably to detect asteroseismic oscillations), dwarf stars later than M7, stars with well-measured properties, etc.
- Prospects for observations relevant to stellar astrophysics, many of which may overlap with exoplanetary science. For instance, we may wish to try and measure a large sample of stellar rotation periods, or allocate a larger fraction of the data mass for short-cadence asteroseismic targets. We may also wish to observe optical/near-IR variable targets across the sky, in particular pulsating stars (Cepheids, RR Lyrae, δ Scuti, slowly pulsating B stars), eruptive stars (protostars, giants, eruptive binaries, flare stars), cataclysmic variables (dwarf novae, novae, supernovae), rotating variable stars (deformed by ellipsoidal variations, showing variability from stellar spots or magnetic fields), and eclipsing binaries.
- Prospects for solar-system science, such as observations of main belt asteroids and the brightest near-Earth asteroids.
- Prospects for extragalactic astronomy and high energy astrophysics; for instance, gathering light curves of variable active galactic nuclei, and extended low surface brightness features of galaxies or of the Milky Way.

Regarding opportunities and risks, the following need to be considered:

Opportunities:

- What's best on a $>$ 1 year horizon? For instance, if it were known in advance that *TESS* would continue operations for several additional years (or even 10 years), would such knowledge affect the optimal choice of the immediate one-year plan?
- Ability to promote targets that were detected in FFIs to PSs in the Extended Mission.
- Shorten the cadence of FFIs & lengthen the cadence of 'target' stars.
- *TESS as follow-up mission:* ability to observe *CoRoT* objects; ability to observe the *Kepler* field; ability to observe *K2* fields (follow-up *K2* few-transit objects); ability to observe targets previously monitored by ground-based surveys.
- *Follow-up for TESS:* potential for *JWST* follow-up, potential for *CHEOPS* follow-up, ability to obtain *TESS* photometry contemporaneously with ground-based observations, ability to follow up with resources in both hemispheres.
- Impact on Guest Investigator program.

Risks: Risk of spacecraft damage. Risk of not meeting threshold science (however it is defined for the Extended Mission). Risk of excessive false positives, for instance from crowding. Would partial instrument failure in Primary Mission make this scenario infeasible? Would reduced precision (from aged CCDs, worse pointing accuracy, or other mechanical sources) invalidate this scenario? Risk of planet detection simulation ~~over~~ or under-estimating planet yield.

1.4 *Description of planet detection model*

Sullivan et al. [2015] (hereafter, S+15) developed a simulation of *TESS*'s planet and false positive detections based on the spacecraft and payload design specified by Ricker et al. [2014]. We adapt this simulation for Extended Mission planning. With our additions, we can change where *TESS* looks in additional years of observing while holding fixed all other mission-defining parameters. Our approach is to run our planet detection simulation for each plausible pointing strategy, and to compare the relative yields of detected planets. This lets us compare Extended Mission scenarios with one another and with the Primary Mission.

Background on synthetic catalogs: *TESS* is sensitive to sub-Neptune sized transiting planets orbiting M dwarfs out to $\lesssim$ 200pc and G dwarfs out to $\lesssim$ 1kpc (S+15, Sec. 2.3). It is sensitive to giant planets and eclipsing binaries across a significant fraction of the galactic disk. With this sensitivity in mind, the stellar catalog we 'observe' in our planet detection simulation is drawn from the output of TRILEGAL, a population synthesis code for the Milky Way [Girardi et al., 2005]. S+15 made some modifications to the catalog, notably in the M dwarf radius-luminosity relation, to better approximate interferometric stellar radii measurements. We retain these modifications; the modified TRILEGAL stellar catalog shows acceptable agreement with observations[2], specifically the Hipparcos sample [Perryman et al., 1997, van Leeuwen, 2007] and the 10pc RECONS sample [Henry et al., 2006].

With a stellar catalog defined, we populate the stars in the catalog with planets based on occurrence rates derived from the *Kepler* sample. We use rates Fressin et al. [2013] found for planets orbiting stars with $T_{\rm eff} > 4000$K and those that Dressing and Charbonneau [2015] found for the remaining M and late K dwarfs.

Detection process: We then simulate transits of these planets. Assuming the transit depth and number of transits are known, we use a model of *TESS*'s point spread function (PSF) to determine optimal photometric aperture sizes for each postage stamp star (*i.e.*, we compute the noise for all plausible aperture sizes, and find the number of pixels that minimizes this noise). With the aperture sizes and noise corresponding to a given integration time known, we compute a signal to noise ratio for each transiting object. Our model for planet detectability is a simple step function in SNR: if we have two or more transits and SNR > 7.3, the planet is 'detected', otherwise it is not[3]. Our model for *TESS*'s photometric precision is described by S+15 and shown in Fig. 7.

Assumptions of SNR calculation: Our approach to computing SNRs for each transiting object is not time-resolved. In other words, we are not simulating every 2 second CCD readout, stacking those hypothetical readouts into 2 minute cadence postage stamps and 30 minute full frames, and then reducing simulated light curves.

Our calculation is simpler. We assume perfect period-recovery, phase folding, and identical conditions between transits. We also assume that we observe a constant transit depth, which is diluted by binary companions and background stars in the same manner between transits. Our approach is then to simply tally the number of *TESS* fields a given host star falls within, which corresponds to a known total observing baseline. Assuming random orbital phasing,

[2] Looking closely at the radius-luminosity relations, we do see non-physical interpolation artifacts. These outliers are visible in Figs. 5 and 6 below, but are a small enough subset of the population that we ignore them for this work.

[3] The value of this threshold is chosen to ensure that no more than one statistical false positive is present in a pipeline search of 2×10^5 target stars. When observing a greater number of stars, for instance in the full frame images, a higher threshold value should be imposed to maintain the same condition. We discuss this further in Sec. 3.3.

we then compute the number of transits *TESS* observes for planets of any given host.

Not clear to me if you estimate N_{tra} analytically or by monte carlo.

Using a model PSF, we determine ideal aperture sizes and obtain an estimated noise per transit, which we can then phase-fold. Summarizing the relevant terms in an equation,

$$\begin{aligned} \mathrm{SNR}_{\mathrm{phase-folded}} &\approx \sqrt{N_{\mathrm{tra}}} \times \mathrm{SNR}_{\mathrm{per-transit}} \\ &= \sqrt{N_{\mathrm{tra}}} \times \frac{\delta \cdot D}{\left(\frac{\sigma_{1\mathrm{hr}}^2}{T_{\mathrm{dur}}} + \sigma_v^2\right)^{1/2}}, \end{aligned} \tag{1}$$

for δ the undiluted transit depth; D the dilution factor computed from background and binary contamination (Eq. 3); $\sigma_{1\mathrm{hr}}$ the summed noise contribution from CCD read noise, photon-counting noise from the star, a systematic 60 ppm $\cdot$ hr$^{1/2}$ noise floor, and zodiacal noise; T_{dur} the transit duration in hours, and σ_v the intrinsic stellar variability (cf. S+15 Sec 3.5). The first equation is approximate because we do not show the small contribution to the SNR from occultation signals[4]. Note that our only "red noise" contribution is from stellar variability, which following S+15 we assume to be independent over transits and also independent of the duration of a given transit. Given the SNR per transit, this lets us 'phase-fold our light-curves' (light-curves which are never explicitly computed point-by-point) by simplying multiplying the SNR per transit by the square root of the number of transits observed.

[4] We account for this in our simulation by taking a quadrature sum of both transit (shown) and occultation (not shown) signals. This matters only for the case of eclipsing binaries, which we ignore in this work.

Leave this out to K.I.S.S.

We have changed other aspects of this simulation since S+15 was published, and describe these changes in the appended Sec. B.

1.5 *Selecting target stars (and full frame images)*

For the Primary Mission, *TESS*'s short cadence (2 min) targets will be drawn from a subset of the *TESS* Input Catalog. The prioritization statistic that the mission will use in this selection has yet to be explicitly defined.

We know that for *TESS* to detect small transiting planets it should observe stars that are small and bright. For this work, we define a simple statistic, `Merit`, proportional to the SNR we should expect from an arbitrarily sized planet orbiting any star:

$$\texttt{Merit} \equiv \frac{1/R_\star^2}{\sigma_{1\text{-hr}}(I_c)/\sqrt{N_{\mathrm{obs}}}}, \tag{2}$$

where $R_\star$ is the radius of the star in question, $\sigma_{1\text{-hr}}$ is the relative precision in flux measurements over one hour of integration time, taken from an empirical fit to Fig 7, I_c is the Cousins band I magnitude *TESS* observes for the star (or more precisely, the star system) and

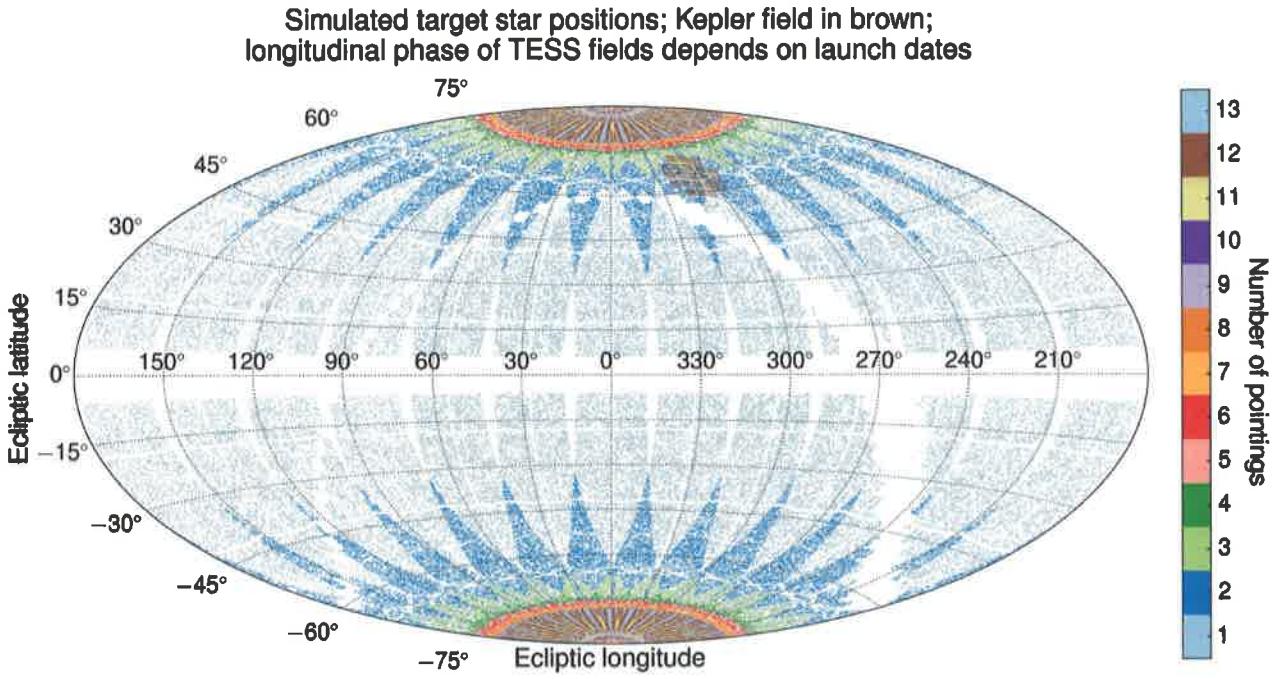

Figure 4: Selected target stars in the Primary Mission. Their density increases towards the poles because of the $\sqrt{N_{\rm obs}}$ weight in selection. Dead space on the CCDs creates 'gaps' in the continuous viewing zones.

what?

$N_{\rm obs}$ is the number of observations the star receives over the course of the mission. For multiple star systems, $R_\star$ is taken to be the radius of the planet-hosting star, and the I_c magnitude is based on the combined flux from all the stars.

We evaluate `Merit` for all the star systems in our modified TRILEGAL catalog, and then choose the best 2×10^5 as target stars to be observed at 2 minute cadence. Target stars selected in this manner are shown in Fig. 4. This statistic is simpler than the procedure outlined in Section 6.7 of S+15 and it produces a nearly identical population of target stars (shown in Fig 5). Our approach for full frame image simulation is different from that of S+15, and we describe it below.

This is an error. Light from the non-host will dilute, not improve, detectability.

"best" means what? largest value of Merit?

We generalize our `Merit` statistic to Extended Missions as follows: over an entire mission, the total number of observations a star receives is the sum of its observations in the Primary and Extended Missions: $N_{\rm obs} = N_{\rm primary} + N_{\rm extended}$. If $N_{\rm extended} = 0$ for a given star, then do not select that star as a target star in the Extended Mission. Else, compute its `Merit` (Eq. 2) ~~weighted by~~ substituting $N_{\rm obs} = N_{\rm primary} + N_{\rm extended}$. In this manner stars that are observed more during the Primary Mission are more likely to be selected during the Extended Mission.

This method doesn't explicity include limits to number of stars on a given camera's field of view, right? I assume you've checked that it isn't advocating for more stars in the pole-looking camera than can be accomodated.

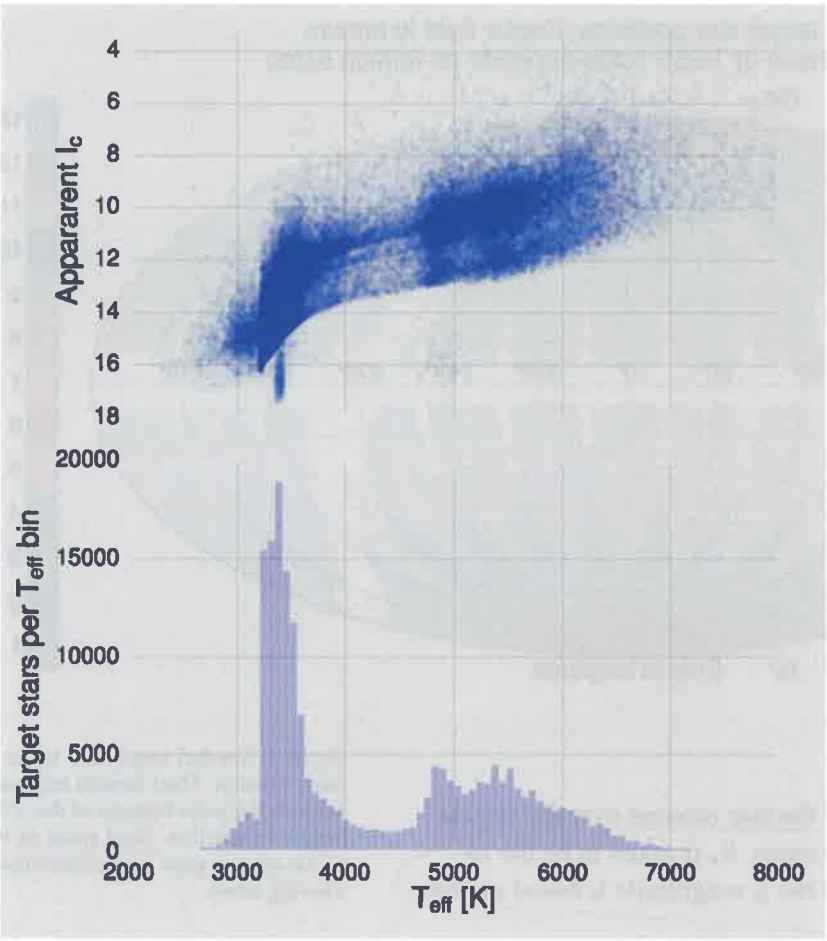

Figure 5: Target star Cousins I magnitude against effective temperature (replicates Figure 17 of S+15). Target stars are selected as the best 2×10^5 stars according to $\texttt{Merit} \equiv \sqrt{N_{\rm obs}}(1/R_\star^2)/\sigma_{\text{1-hr}}(I_c)$. The top subplot shows 1 in 10 stars. This simple model could inform the target selection to be performed on the *TESS* Input Catalog. The lower histogram is bimodal, selecting heavily for M dwarfs, and selecting more F and G dwarfs than K dwarfs. This shape arises from the combined $1/R_\star^2$ and $1/\sigma_{\text{1-hr}}(I_c)$ weights: the fact that the minimum falls around K dwarfs occurs because of both a Malmquist bias (there are more F than K stars of comparable brightness in our catalog from which to select) as well as a corresponding dip in the TRILEGAL (& observed) V-band luminosity functions (see S+15 Figure 5).

Outliers visible in the upper scatterplot are non-physical, possibly artifacts from S+15's Padova-to-Dartmouth interpolation as they tend to have greater masses than all other stars on the main sequence. As they comprise less than 1% of the target stars, we ignore them in order to proceed.

Alternative prioritization approaches: It is worth emphasizing that our scheme for selecting target stars for an Extended Mission does not make use of any information on whether candidate transit events were observed during the Primary Mission. If a star were observed at short cadence for an entire year, and no candidate events were found, it might be sensible to disregard that star in the Extended Mission in favor of stars that have never been observed at short cadence – particularly those with candidate events that were detected in the Primary Mission full-frame images. These and related concerns are discussed further at the accompanying Wiki document[5].

More abstractly, the procedure of simply applying Eq. 2 attempts to select a stellar sample that will yield the most small transiting planets around the brightest stars. An alternative approach would be to select stars that will give the most *relative benefit* in 2 minute postage stamps over 30 minute cadence observations since all stars will be present in the 30 minute images. This 'relative benefit' could

[5] `https://spacebook.mit.edu/display/TESS/Extended+Missions`

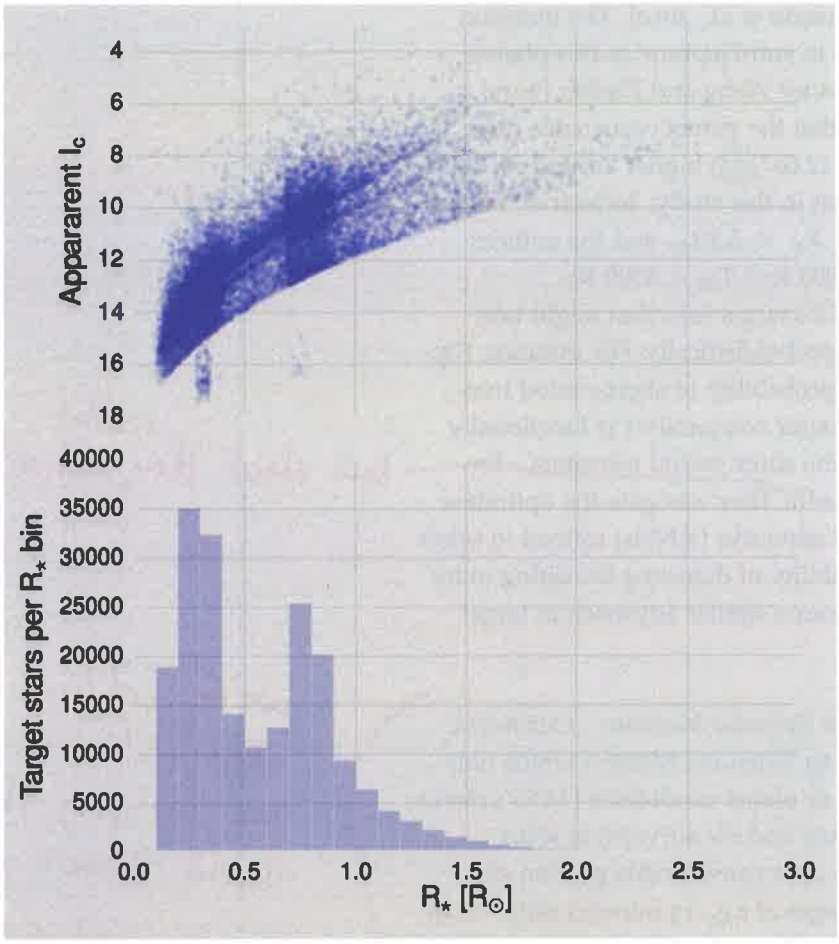

Figure 6: Same as Fig. 5, but as a function of stellar radius. $1/R_\star^2$ selection weight clearly visible, along with the same outliers.

be based on improvement in transit detectability, or perhaps improved capacity to resolve the partial transit phases.

For purposes of transit detection, the difference between 2 and 30 minute cadence matters most when transits have short durations – in other words for small stars, and for close-in planets. Switching to this alternative approach would consequently bias us even more strongly towards selecting M dwarfs. We already select almost every M dwarf with $I_c < 14$. The limiting I_c magnitude for detecting $R_p > 4R_\oplus$ planets with *TESS* is ~ 16, which is where we see the dimmest stars in Fig. 5.

Additionally, the procedure of applying Eq. 2 and assuming that it will maximize the number of small planets that *TESS* will detect about bright stars ignores the functional dependence of planet occurrence rates on stellar properties. For instance, should we prioritize target stars that are metal-rich? Metal-rich stars demonstrably host more giant planets within *TESS*'s period sensitivity than metal-poor

stars [Fischer and Valenti, 2005, Johnson et al., 2010]. The question of whether this correlation extends to sub-Neptune radius planets is somewhat contested, but for instance Wang and Fischer [2015] used a sample of KOIs and found that the planet occurrence rates of (gas dwarf) planets are $1.72^{+0.19}_{-0.17}$ ($2.03^{+0.29}_{-0.26}$) higher around metal-rich than metal-poor stars. Note that in this study, 'terrestrial' means $R_p < 1.7R_\oplus$, 'gas dwarf' $1.7R_\oplus < R_p < 3.9R_\oplus$, and the authors focused only on solar-type stars (4800 K $< T_{\rm eff} <$ 6500 K).

A more robust approach for *TESS*'s target selection might take these kinds of results into account probabilistically. For instance, Kipping and Lam [2016] note that the probability of short-period transiters having additional transiting outer companions is functionally dependent upon the properties of the short period transiters – for instance their orbital periods and radii. They navigate the optimization problem using artificial neural networks (ANNs) trained to select for features that improve the probability of detecting transiting outer companions. *TESS* might benefit from a similar approach in target selection.

how about their orbital inclinations?

Alternative prioritization approaches in Extended Missions: Our `Merit` statistic also neglects the option of an Extended Mission which only observes stars with known planets or planet candidates (*TESS*'s objects of interest, or those from other transit and RV surveys) at short cadence. This approach would free up a considerable portion of *TESS*'s data mass for full frame images at *e.g.*, 15 minutes rather than the current nominal 30 minutes.

we're getting into alternatives. Is it too early in the paper? Should these go into the discussion section?

Approach to full-frame images: We want to simulate the full frame image detections in a computationally tractable manner. While S+15 evaluated the phase-folded SNR for every potentially transiting object about each of the $\sim 1.6 \times 10^8$ stars in our synthetic catalog, we focus only on the stars for which *TESS* could plausibly detect a sub-Neptune planet over the 3-year mission. Most stars that *TESS* sees are too dim or too large to detect $R_p < 4R_\oplus$ planets – while we expect many giant planet detections towards the galactic plane (S+15 Fig 19), small-planet detections are more nearly isotropic, since practically all occur for stars at $<$ 1 kpc. For our purposes in this study, we argue that knowing there will be thousands of giant planet candidates is sufficiently accurate. The prospects for detecting smaller planets are more likely to help discriminate between different scenarios for the Extended Mission.

In this vein, we only simulate full frame image detections for the 3.8×10^6 highest `Merit` stars following the 2×10^5 highest `Merit` stars observed as 'postage stamps'. This number (3.8×10^6) was initially

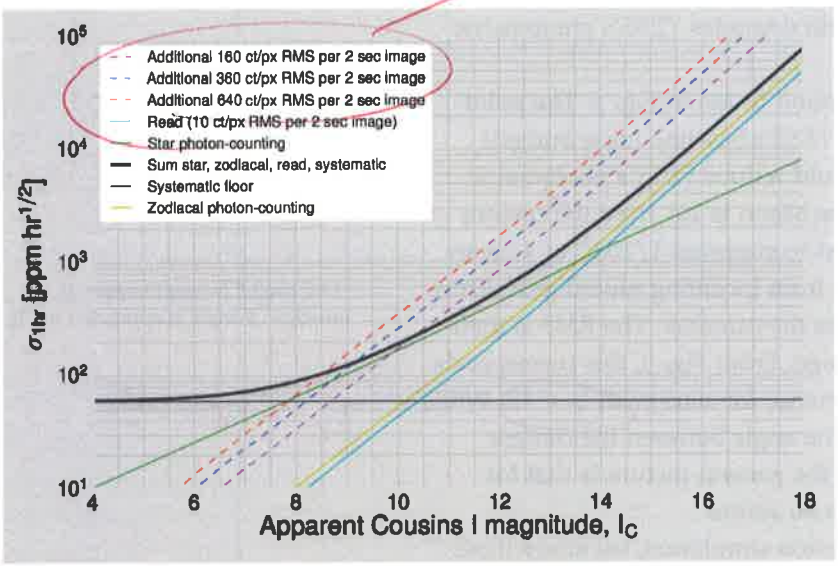

Figure 7: Relative precision in measured flux over a one hour integration time (scatter from contaminating background stars and PRF centroid offsets ignored). The noise sources described by Sullivan et al. [2015] are solid thin lines. The dashed lines exemplify noise from contaminating background flux, for instance from the Moon or Earth outside the *TESS* field, but still scattering light off the *TESS* lens hood. A dynamical 3-body simulation lets us estimate the impact lunar and Earth backgrounds have on *TESS*'s photometry. The photometric precision with which we simulate observations has additional scatter about the thick black line owing to randomly-assigned contaminating stars. Zodiacal background is plotted for an ecliptic latitude of 30° following Sec. 6.4.1 of Sullivan et al. [2015]

estimated based on the number of searchable stars about which we expect *TESS* to be able to detect sub-Neptune radius planets [Winn, 2013b]. The detection process is then identical to that for postage stamps, except with 30 minute instead of 2 minute exposures, which increases the apparent durations and shrinks the apparent depths for transits with durations of $\lesssim$ 1 hour. To ensure that 3.8×10^6 stars is sufficient to include all stars about which *TESS* might detect sub-Neptune radius planets, we repeated this process for the Primary Mission using 5.8×10^6, 9.8×10^6 and 19.8×10^6 'full frame image' stars, and confirmed that there was no significant difference in the planet yields at $R_p \leq 4R_\oplus$ between any of the cases. Increasing the number of FFI stars, the runs yield increasing numbers of giant planets, particularly near the galactic disk. Meanwhile the number of sub-Neptune radius planets remains fixed, and thus convinces us that our simulation includes a sufficient number of target stars to be complete for sub-Neptune detection statistics.

1.6 *Earth and Moon crossings*

When the Earth or Moon passes through *TESS*'s camera fields they can flood the CCD pixels to their full well capacity ($\sim 2 \times 10^5$ photoelectrons). Precision differential photometry becomes impossible in any pixels that are directly hit during these crossings. Even when the body (Earth or Moon) is not directly in the camera's field of view, its light scatters off the interior of spacecraft's lens hood and acts as a background source of contaminating flux across many of the cameras[6]. The Poisson noise in the number of photons arriving from the

[6] A detailed model for this process is not yet available.

Earth or the Moon in such a scenario degrades *TESS*'s photometric performance.

We show a few example background fluxes in Fig. 7. The point of this figure (aside from showing *TESS*'s baseline noise budget) is that additional scattered light could reduce *TESS*'s photometric performance. For instance when the Moon is 24° from the camera boresights the lens hood is expected to suppress $1/100^{\text{th}}$ of a mean 3×10^6 ct/px (per 2 second image) from incoming moonlight[7]. Thus a mean flux of 3×10^4 ct/px reaches the cameras. The RMS is then roughly 173 ct/px per 2 second image. From Fig. 7, this corresponds to $\gtrsim 3\times$ worse photometric performance for stars with $I_c < 12$. While this effect is highly dependent on the angle between the camera boresights and the Moon or Earth, the general picture is that for field angles $\theta \lesssim 25°$, the impact can be severe.

[7] Our model for suppression as a function of angle is appended in Fig. 25

Separately from our planet detection simulation, we study these crossings in a dynamical simulation based on JPL NAIF's standard SPICE toolkit. Given a nominal launch date, this code determines *TESS*'s orbital phasing throughout its entire mission. At every time step of the three-body orbit, we calculate the distance between *TESS* and the other two bodies of interest, and the separation angles among each of the four cameras and each of the two bodies (eight angles in total). The gravitational dynamics behind this calculation treat the Earth, Moon, and Sun as point masses, and the *TESS* spacecraft as a massless test particle. The spacecraft's inclination oscillates in the simulation as it will in reality.

Taking the Earth and Moon's integrated disk brightnesses as fixed values[8] we use a model for scattered light suppression from the *TESS* lens hoods (Fig. 25) to compute the mean photon flux from each of these bodies onto each of the cameras throughout the orbit. We then compute the corresponding variance in incoming flux, and compare it to *TESS*'s noise budget.

[8] The full moon's apparent magnitude is $I_\mathbb{D} \approx -13.5$. Scaling from photon fluxes tabulated in Winn [2013a], this gives 2.5×10^{13} ct/s. Averaging over the focal plane array, this gives a mean additional flux per image of 3×10^6 ct/px. The relevant variance is (roughly) the square root, ≈ 1730 ct/px per 2 sec image. The Earth is roughly $80\times$ brighter, and so will contribute an RMS $\sqrt{80}$ times greater: ≈ 15500 ct/px per 2 sec image. This substantiates the claim that the Earth and Moon flood the cameras to their full well capacity. The effect on observing precision is appended in Fig. 26.

To evaluate the cumulative impact of Earth and Moon crossings on *TESS*'s Primary and Extended Missions we ask: for each camera, what fraction of the total observing time is *TESS* unable to operate at desired photometric precision because of Earth and Moon crossings? An upper limit for what we mean by 'unable to operate at desired photometric precision' is when terrestrial or lunar flux make it impossible to observe a sizable portion of the stars in the *TESS* target star catalog with reasonable precision. For example, Fig. 26 shows that ~80% of the stars that could be observed at sub-mmag precision over an hour no longer can when the Earth is 17° from the camera boresight. This of course depends on the target star catalog's apparent magnitude distribution (Fig. 5), and the cutoff of 'sub-mmag precision over an hour' is arbitrarily selected.

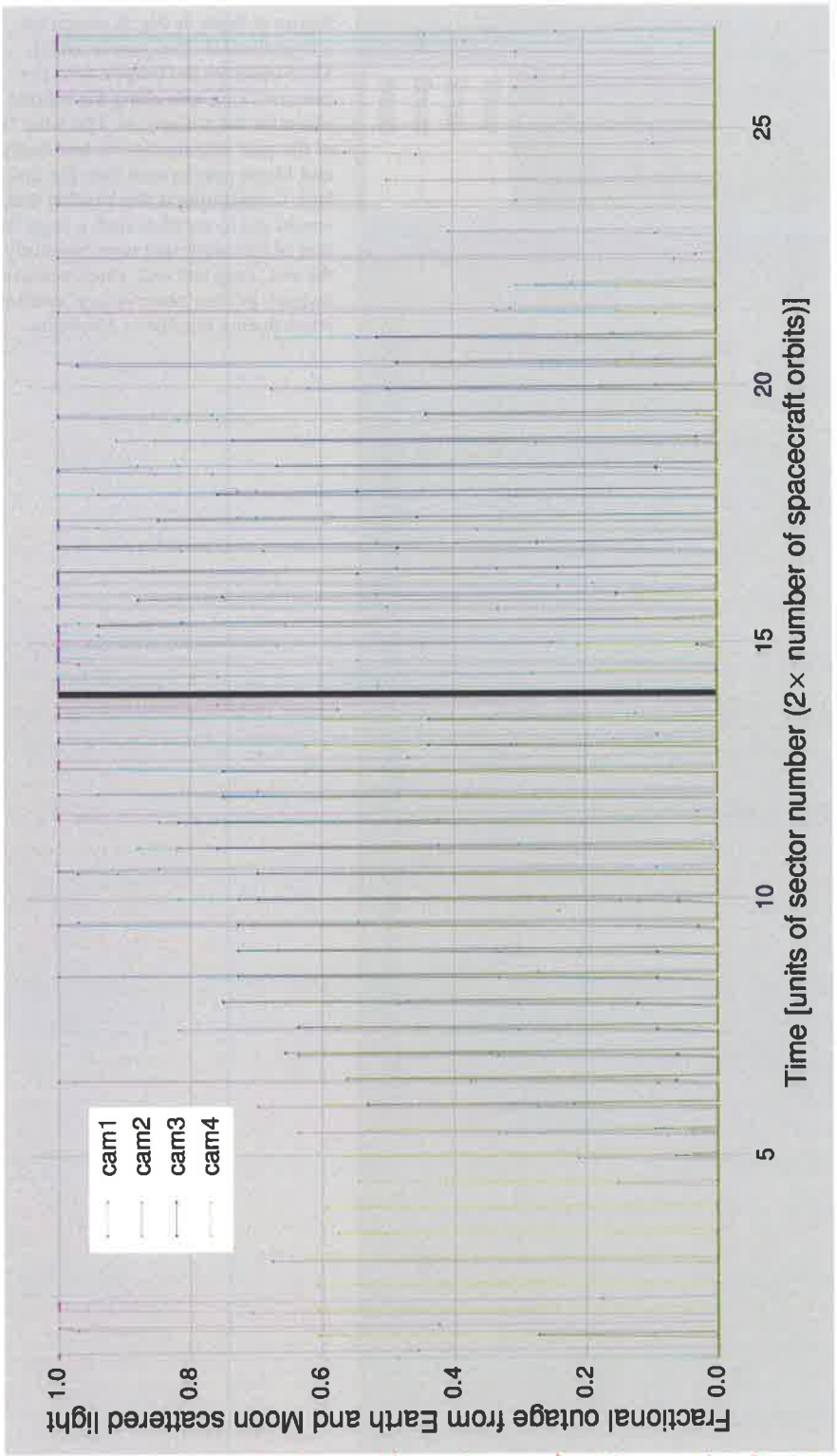

Figure 8: 'Outage' caused by Earth and Moon crossings as a function of time in the orbit. Specifically, the y-axis shows the probability of having a polluted frame with mean incident earthlight or moonlight of > 300 ct/px/s in a time-step bin of $1/20^{\text{th}}$ of an orbit (where the probability is the number of polluted frames divided by the total number of frames in that bin). The mean of this outage across any given year is used to compute the number of dropped fields in Table 1, which should then be an upper bound to the impact of Earth and Moon crossings. In this plot, the first year of observations are in the southern ecliptic hemisphere. The black dividing line indicates the beginning of 'Year 2' (northern hemisphere). The worst fractional outage per orbit is in Camera 1, which points towards the ecliptic, over the first ~ 5 orbits of the second year. The plot has 'spikes' because outage typically only occurs over a small fraction of the orbit of TESS.

Alternative rendering of same

Insert a Grey scale of 4 levels, or stippling of 4 different densities

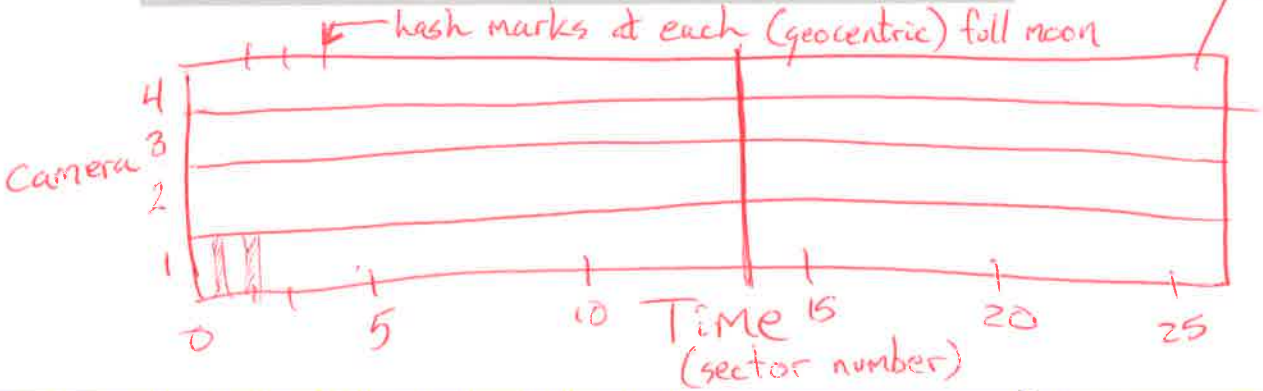

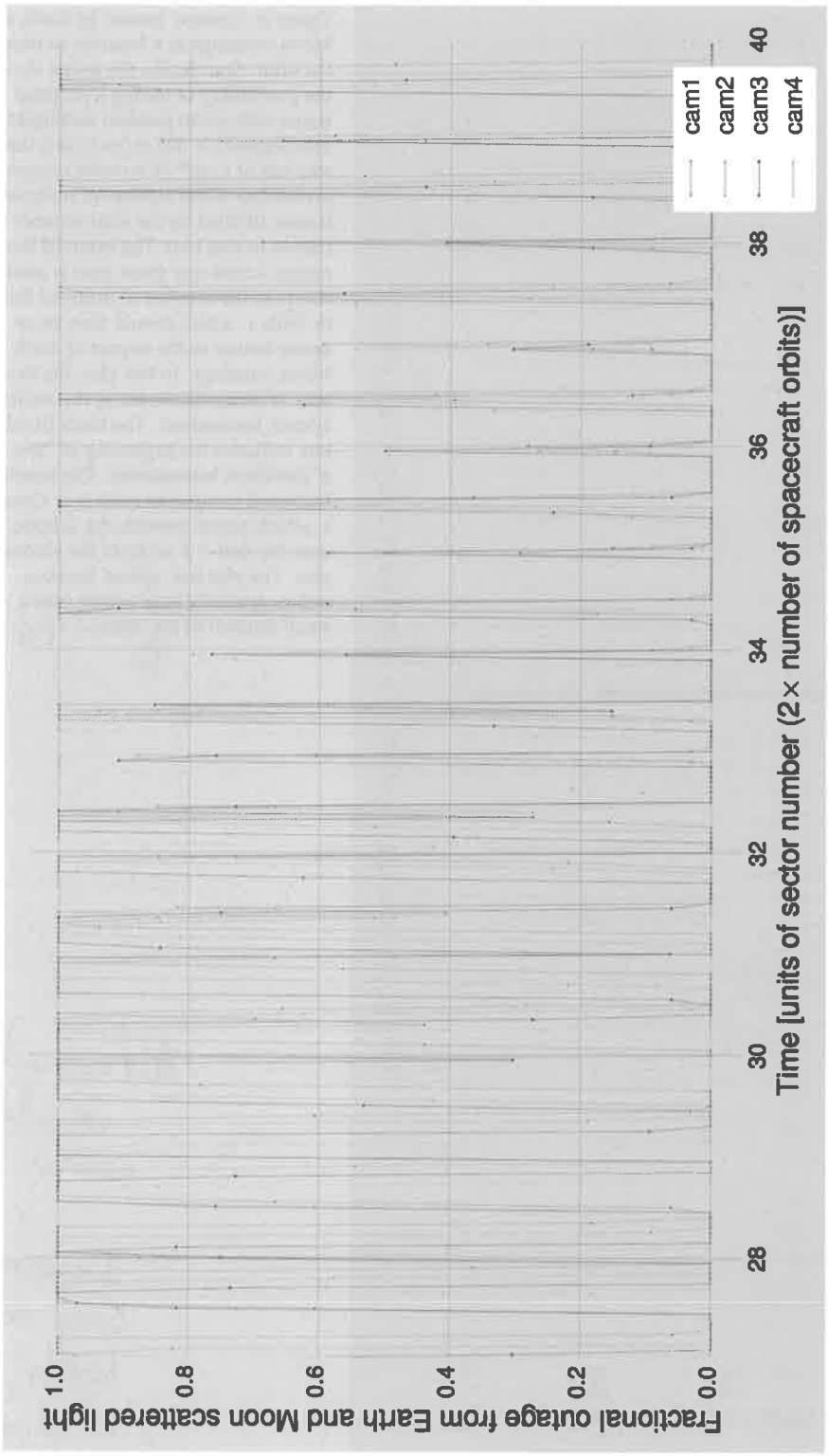

Figure 9: Same as Fig. 8, except for a hypothetical third year in which *TESS* observes the ecliptic with the cameras' long axis along the ecliptic plane for the entire year. The latter half of the year experiences far less Earth and Moon interference than the first half. Considering it implausible that we would opt to sacrifice such a large fraction of our observing time, we study the `ecl_long` and `ecl_short` scenarios instead, as their observations avoid this effect during the first $\sim$ 5 months.

	Camera 1	Camera 2	Camera 3	Camera 4
Year 3 selected				
`pole`	0	0	0	0
`hemi`	2	1	0	0
`hemi+ecl`	2	0	0	0
`ecl_long`	1	1	1	1
`ecl_short`	0	1	1	0
`allsky`	1	1	0	0
Year 3 omitted				
`pole (south)`	0	0	0	0
`hemi (south)`	1	0	0	0
`hemi+ecl (south)`	4	3	0	0
`ecl_long (1yr)`	4	4	4	4
`ecl_short (1yr)`	1	3	4	2
`allsky (poles)`	0	0	0	0
Primary Mission				
`hemi (south year 1)`	2	1	0	0
`hemi (north year 2)`	4	2	0	0

Table 1: Number of sectors (of 13 per year) 'dropped' due to the Earth and Moon crossings in both selected and omitted Extended Missions, with those of the Primary Mission for reference. The method of 'dropping' fields (which neglects the temporal nature of the crossings, discussed in the text) gives an approximate sense of the cumulative impact of Earth and Moon crossings. Scenarios with `(south)` appended refer to their counterparts in the southern ecliptic hemisphere. `ecl_long (1yr)` corresponds to a full year with the *TESS* field's long axis along the ecliptic, and `ecl_short (1yr)` corresponds to the same, but with the short axis along to the ecliptic. These scenarios are neglected because their outages are time-correlated (see Fig. 9). `allsky (poles)` would be a scenario that observes in the manner of `allsky`, but only on the ecliptic poles as in `pole`.

Developing a detailed model of how these crossings impact *TESS*'s photometry is beyond the scope of this work. To account at least qualitatively for their effect in our simulation we adopt a simple approximation: we impose that a camera has an 'outage' if there are over $F_{\text{thresh}} \equiv 300$ cts/px/s (an additional RMS of $\approx$ 25 ct/px per 2 sec image). We then compute the time-averaged fraction of each observing sector for which *TESS*'s cameras remain above this threshold. A given sector has ~ 660 hours of observing time over two spacecraft orbits. As an example, suppose that 220 of these hours had the Earth, the Moon, or both shining with a background flux $F > F_{\text{thresh}}$. This would correspond to a fractional outage of 1/3. We then compute the mean of this fractional outage across all 13 annual sectors to derive a 'mean camera outage' for each proposed pointing scenario. We then approximate the effect of Earth and Moon crossings by selectively omitting the closest integer number of observing sectors corresponding to the 'mean camera outage' described above. For instance, if the 'mean camera outage' was 17% of *TESS*'s observing time over a given year, we would omit the 2 (of 13) observing sectors that suffer the greatest number of lost hours, for that given camera. The relevant number of omitted sectors is shown in Table 1; an example of the resulting spatial distribution of detected planets is shown in Fig. 11.

As mentioned in Sec. 1.4, our planet detection simulation is not explicitly time-resolved; it takes the ecliptic coordinates of camera

fields for each orbit as input to compute the observed baselines for each star in our galactic model. While our procedure ignores the temporal nature of the 'outages' (which is shown resolved over time-steps of $1/20^{\text{th}}$ of an orbit in Figs. 8 and 9), it gives a sense of the cumulative impact of Earth and Moon crossings over the course of a year.

Our approximation is 'conservative' in the sense that the additional background corresponding to $F_{\text{thresh}} = 300$ ct/px/s only becomes a noticeable noise source for targets with spectral types later than M0 at $I_c \lesssim 14$ (see appended Fig. 27 and cross-reference Fig. 5). This corresponds to a relatively small fraction of stars in the input catalog (18%), which are observed with $\lesssim 1.5\times$ worse precision. By counting all the relevant time as an 'outage' lost across all stars (even the bright ones for which the additional scatter is subsumed by shot-noise), our simulation results are likely more sensitive to scattered light than *TESS* will be in reality.

The impact of this approximation on the planet yields of the Primary and Extended Missions are discussed in Secs. 2.1 and 2.3 respectively. The summarized result is that this model of Earth and Moon crossings leads to $\lesssim$10% fewer $R_p < 4R_\oplus$ planet detections compared to the case of not accounting for the crossings at all. There is thus little reason to raise our low threshold, given that the magnitude of the effect is so small. Moreover, the Earth and Moon crossings typically last for a small fraction of an orbit (Fig. 8). If the timescales required for the cameras to 're-settle' after the crossings are small compared to orbital timescales, our approach may over-estimate the effect's importance even further. Detailed models of this process remain to be developed during the spacecraft's commissioning period.

1.7 *Summary of key assumptions and attributes of the planet detection simulations*

- We focus almost exclusively on planets with $R_p < 4R_\oplus$.
- We assume the TRILEGAL catalog (modified to match interferometric radii, as described by S+15) is an accurate representation of the stellar neighborhood to $\lesssim$ 2kpc.
- We omit the 5% of the sky closest to the galactic disk (see Fig. 4). We expect that *TESS*'s large pixel size ($21 \times 21''$) combined with crowding near the galactic disk will cause substantial source confusion and a large astrophysical false positive rate in this area. On a practical note, TRILEGAL cannot be queried within its run-time limit for some of these fields (cf. S+15 Sec 3.1).
- We assume prior knowledge of the radii and apparent magnitudes

wrong. see Fig 27 comments

On the flip side, the effect of scattered light could be non-Poisson* and thus MUCH worse than simulated.

* imagine a time-variable gradient** wafting across each focal plane as the moon (or Earth) moves relative to TESS's pointing.

** and then a "splatter" instead of a smooth gradient.

of TRILEGAL's synthetic stars, so we can prescribe a simple prioritization statistic (Eq. 2) that we expect (but have not verified) maximizes the number of small planets we discover about bright stars[9].

- In evaluating a star's `Merit` (Eq. 2), we assume an observed magnitude for each star that comes from the sum of the flux from the star itself in addition to any companion and background stars (whose presence will not be known by the mission a priori, but which we then account for when computing 'observed' SNRs).
- We use occurrence rates of planets as a function of radius and orbital period as calculated by Fressin et al. [2013] and Dressing and Charbonneau [2015]. We assume these are accurate for the $P \lesssim 180$ day planets to which *TESS* is sensitive.
- The occurrence statistics of multiple-planet systems can approximated as repeated independent draws from the single-planet distributions. The orbits of planets in multiple planet systems are coplanar and stable (with period ratios of at least 1.2 between adjacent planetary orbits).
- For our instrument and noise models, we assume:
  - A point-spread function (PSF) derived from ray-tracing simulations, slightly degraded from that described by S+15 Sec 6.1, and based on laboratory measurements.
  - All stars are observed at the *center* of the *TESS* CCDs. This ignores off-axis and chromatic aberrations within the *TESS* optics, and consequently ignores the angular dependence of the pixel response function (the fraction of light from a star that is collected by a given pixel). While S+15 attempted to model the field-angle dependence, we argue that the methodology used in that work was inconsistent (see appendix Sec. B), and that rectifying this approach would be complex and time-consuming. Ignoring the field-angle dependence is a simplification that may lead to loss of accuracy, but since this applies to all the scenarios under consideration, it should still be possible to *compare* the results of different scenarios without much loss of accuracy.
  - The time/frequency structure of all noise (except for stellar variability, see Eq. 1) is 'white'. This means that we ignore time-correlated instrumental effects such as spacecraft jitter, thermal fluctuations, and mechanical flexure, which we expect will be at least partly mitigated by the mission's data reduction pipeline.
  - We assume the instruments work equally well in year 3 as in years 1 and 2.

[9] Although it is difficult to determine accurate photometric radii, we expect that by the time *TESS* launches *Gaia* will provide parallaxes and proper motions for many *TESS* targets, allowing *TESS* to discriminate between red dwarfs and red giants for purposes of target prioritization.

- The assumed contributors to white noise include: CCD read noise, shot noise from stars, a systematic noise floor of 60 ppm $\cdot$ hr$^{1/2}$, and zodiacal background. See Fig. 7 for the relative contributions of these terms as a function of apparent magnitude.
- The noise contributions from stellar intrinsic variability are assumed to be identical to those described by S+15 Sec3.5, which uses variability statistics from the *Kepler* data computed by Basri et al. [2013]. Unlike all previously mentioned noise sources, we do not scale noise from stellar variability as $t_{\rm obs}^{-1/2}$, since the photon flux from stars may vary over time-scales similar to typical transit durations. Instead, we assume the noise contribution from stellar variability is independent across transits, and thus scales as $N_{\rm tra}^{-1/2}$, for $N_{\rm tra}$ the number of observed transits.

- For our detection model, we assume:
  - A step-function detection threshold: for SNR $\geq$ 7.3, we rule transiting planets as detected, for SNR $<$ 7.3, they are not detected.
  - The top 2×10^5 merit-ranked targets (Eq. 2) are observed at two-minute cadence, and the next 3.8×10^6 stars are observed at thirty-minute cadence. We use S+15 Sec. 6.8 approach to 'blurring' transits with durations $\lesssim$ 1hr, so that for longer cadence images shorter transits get shallower depths and longer apparent durations. As described in Sec. 1.5, we verify that under this assumption, our selection of PS stars is nearly complete for all detectable planets with $R_p < 4R_\oplus$, and it is highly incomplete for Jupiter-sized planets.
  - We require $\geq$ 2 transits for detection. We assume the period can be recovered without ambiguity and likewise there is no ambiguity in identifying which target star is exhibiting a given transit signal.
- We do not assume any prior knowledge of previous observations that may have been performed on our stars. For instance, observing the ecliptic, we do not simulate the *TESS-K2* overlap.
- For Earth and Moon crossings, we assume we can drop a fixed number of orbits of observing time for the cameras that suffer most from the Earth, the Moon, or both being in *TESS*'s camera fields. We summarize this effect in Table 1. Although this ignores the time-correlated nature of the outages shown in Figs. 8 and 9, it is sufficient for comparing detected planet yields across missions, and leads to $\lesssim$10% fewer $R_p < 4R_\oplus$ planet detections compared to the case of not accounting for the crossings at all.

put this first, as it is the simplest and most fundamental.

refer back to §1.4 and the set off Eqn I suggest there.

Also SNR is ambiguous here (per transit or combined?)

account for

- We assume that we can (eventually) discriminate between astrophysical false positives (for instance background eclipsing binaries or hierarchical eclipsing binaries) and planet candidates.
- We can compute SNR with effective signal $\delta_{\rm eff} = \delta \times D$ for $\delta = (R_p/R_\star)^2$ the transit depth, and

$$D = \frac{\Gamma_T}{\Gamma_N + \Gamma_T} \tag{3}$$

where D is the dilution factor of a target star with incident photon flux Γ_T from the target star and incident photon flux Γ_N from neighboring stars (*i.e.*, background stars or binary companions).

The noise is computed by creating a synthetic image for every host star with a planet that transits above a 'pre-dilution' SNR threshold (this threshold is imposed for the sake of lowering our computational cost). This 16 × 16 pixel image is of the number of photoelectrons *TESS* sees from the star and its companions/background stars at each pixel of each CCD. We produce it through our PRF model, which in turn requires the host star's $T_{\rm eff}$ and apparent I_c. Over each image, the noise is computed for a range of possible aperture sizes about the brightest pixel (see S+15 Secs. 6.2 and 6.3), and then finally a single 'noise' for each transit is selected by choosing the aperture size that minimizes the noise.

2 *Planet detection statistics*

Using the planet detection model described in Sec. 1.4 and the target selection procedure of Sec. 1.5, we simulate three years of *TESS* observing, for six different possibilities for the third year: `hemi`, `pole`, `hemi+ecl`, `ecl_long`, `ecl_short`, and `allsky`. How many new planets do we detect, and how do their properties differ between Extended Missions?

2.1 *Planet yield from the Primary Mission*

We first examine our results for just the Primary Mission – the first two years of *TESS*'s observing. We follow with an analysis of our detected planet populations from a single Year-3 Extended Mission (Sec. 2.2), and then all six of our proposed Extended Missions (Sec. 2.3). Here we highlight commonalities and differences between S+15 and this work.

Detected planet yield The first point of consideration is the detected planet yield, shown in Fig. 10. The number of Earths, super-Earths, and sub-Neptunes we detect agrees with the numbers quoted

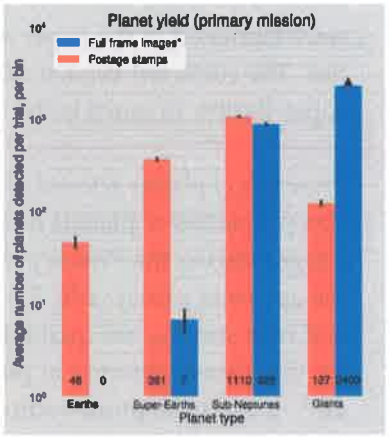

Figure 10: Mean numbers of planets detected in *TESS*'s Primary Mission. The number of Earths ($R_p < 1.25R_\oplus$), super-Earths ($1.25R_\oplus \leq R_p < 2R_\oplus$), sub-Neptunes ($2R_\oplus \leq R_p < 4R_\oplus$) and giants agree with the respective values quoted in Sullivan et al. [2015] to $\lesssim$ 50%. Our full frame images detections in are complete for $R_p < 4R_\oplus$, and incomplete for giant ($R_p > 4R_\oplus$) planets, shown with a lower limit (see text for discussion). Error bars are from only Poisson fluctuations and do not account for systematic uncertainty.

by S+15 to within 50%, despite the modifications described in Sec. 1.5 to the target selection procedure. Other changes to our simulation's assumptions, for instance using an as-built model of *TESS*'s PSF informed by laboratory tests (courtesy Deborah Woods) rather than the idealized PSF described in Sec6.1 of S+15, had minor only impact on this final result ($\lesssim$ 10% change in yield).

A modification that did influence our lowered expected yields was a bug-fix in S+15's dilution calculation. Recall our definition of the dilution parameter D (Eq. 3): placing a binary companion with luminosity identical to the host star into a system with a transiting planet that would typically transit with depth δ leads to a transit with 'effective depth' $\delta/2$. A single missing symbol[10] led S+15 to under-account for this effect, which in our simulations brought about factors of 1.5×, 1.3×, and 1.2× fewer Earths, super-Earths, and sub-Neptunes respectively. This error can be noted in the published Table 6 of S+15, in which nearly all the dilution parameter values are near 1.

[10] An = rather than a +=

cite S+15 erratum

An additional note is that in the preparation of this report, a glaring discrepancy emerged between our predicted $\approx$ 400 super-Earth detections and those shown in Fig. 18 of S+15, which displays $\approx$ 1400 planets. The subsequent investigation led to the discovery of a bug in the plotting script used to create Fig. 18. The error did not affect any of the results described in the text, or the simulation results that were tabulated in the paper and sent electronically to interested parties. The corrected version of S+15's Fig. 18 shows $\approx$ 500 expected super-Earths, in much better agreement.

note also that $\frac{500}{400} = 1.25$

1.25 ≈ 1.3× here

Properties of planets detected in Primary Mission We show the population properties of planets detected in postage stamps and full frame images during the Primary Mission in Figs. 12 and 13. In terms of the apparent planet radii R_p, orbital periods P, host star brightness, and host star $T_{\rm eff}$, we qualitatively agree with the results of S+15 for the planets detected in postage stamps. For instance, the dearth of $P < 5$ day Neptune-radius planets in Fig. 12 was observed by *Kepler* [Mazeh et al., 2016], and thus it is present in our input occurrence rates, rather than being an observational bias. It was also seen by S+15.

remind us: what is Neptune's $R_p/R_\oplus$ value?

The differences between planets detected in postage stamps vs. in full frame images follow our expectation from our `Merit` statistic. Namely, Fig. 13 shows that at a fixed brightness, full frame image detections tend to occur at larger stellar effective temperature (and thus stellar radius). At a fixed host star radius, postage stamp detections occur around brighter stars.

Impact of earth and moon crossings on Primary Mission's detected planet yield During the Primary Mission, of the four cameras Camera 1 (closest to the ecliptic) suffers the most from earth and moon crossings. As noted in Table 1, we remove 4 of its 13 'observing sectors' from that year. This reduces the number of planet detections near the ecliptic, and is visible in the orange points of Fig. 11. In the Primary Mission *TESS* detects $\sim$ 20 planets with $R_p < 4R_\oplus$ from both 2 minute and 30 minute data in each 24° $\times$ 24° camera field nearest to the ecliptic (where each field is observed for 2 *TESS* orbits). As implemented in our simulation, Earth and Moon crossings result in fields simply not being observed, so in these cases planets orbiting stars in these fields are never detected. Considering only the Primary Mission, we would naively expect that dropping a total of 9 fields over the two years (again, see Table 1) would result in a loss of $\sim 9 \times 20 = 180$ planets. This agrees with what our simulations actually give: running them without accounting for Earth and Moon losses returns a mean of 2678 detected planets with $R_p < 4R_\oplus$, while running them with Earth and Moon crossings gives a mean of 2482 such planets (a loss of 196 planets; 7% of the $R_p < 4R_\oplus$ planet yield).

2.2 *Planet yield from an example Extended Mission:* `hemi`

Before comparing our six selected Extended Mission scenarios simultaneously (Sec. 2.3), we describe the detected planet populations from a single realization of an Extended Mission. As an example case, we choose the `hemi` scenario.

A sky map showing the positions of detected planets for this mission is drawn in Fig. 11. Commenting on this map, we note that:

- Any planet detected in this scenario's Primary Mission is also detected in its Extended Mission.* We consequently color the detected planets depending on if they are discovered in the Primary Mission, or whether they are detected only by virtue of the extra data collected in the Extended Mission. In our simulation, these extra observations will lead to new detections (a) because of an increased number of observed transits leading to a higher phase-folded SNR, which causes the transiting object's SNR to clear our threshold of 7.3, and/or (b) because raising the number of observed transits clears the minimum number of transits we require for detections ($N_{\rm tra} \geq 2$).

- The 'dropped' fields described in Sec. 1.6 owing to Earth and Moon crossings are visible for both the Primary and Extended Missions in the $\lambda = (30°, 0°, 330°, 300°)$ fields.

In addition to examining the positions of the detected planets, we

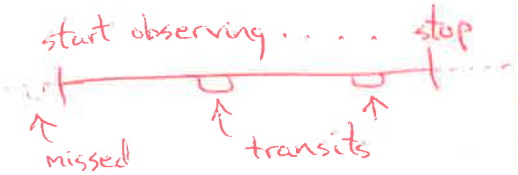

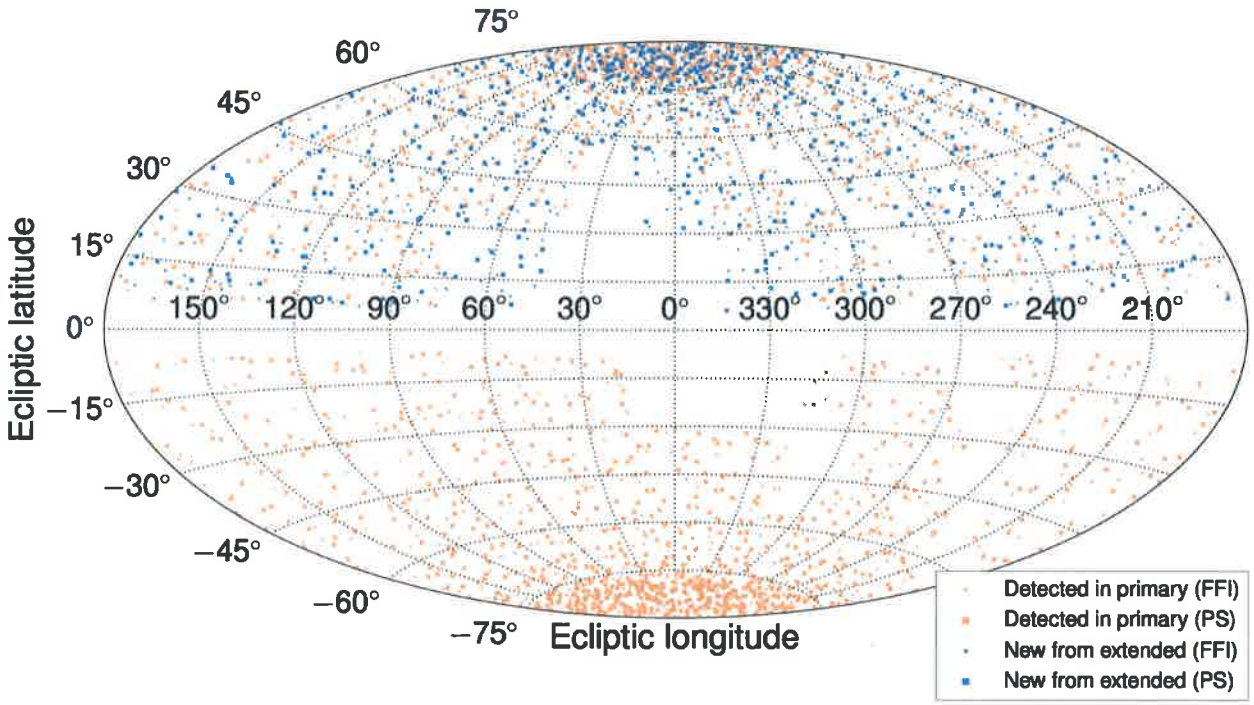

Figure 11: Positions of $R_p < 4R_\oplus$ planets detected in the `hemi` scenario. Squares (postage stamps) and dots (full frame images) are observed at 2 and 30 minute cadence respectively. Orange denotes detection over the first two years of observing (the Primary Mission), and blue denotes newly detected planets from the extra third year. The 'gaps' in fields due to Earth and Moon crossings during the Primary and Extended Missions are noted in Table 1. For instance, the field centered at $(\lambda = 330°, \beta = 18°)$ is observed in the Extended but not the Primary Mission.

select and plot some of their key properties: planet radius R_p, orbital period P, apparent magnitude I_c, and effective temperature $T_{\rm eff}$. See Figs. 12 and 13. Both of these figures are visualizations from a single Monte Carlo realization of the `hemi` scenario, and only show planets with $R_p < 4R_\oplus$. These plots clarify a few points:

- At a fixed period, Extended Missions help us detect smaller planets; at a fixed radius, they let us probe out to longer periods. This is one of the major reasons to extend *TESS*'s observations.
- Almost all $R_p < 2R_\oplus$ planets are detected in postage stamps, not full frame images. This is an indication that the top 2×10^5 `Merit` stars are a sufficient sample to detect most of the $R_p < 2R_\oplus$ planets that *TESS* can detect.
- Postage stamp detections are biased towards M dwarfs. Per Fig. 5, this is largely because our selection procedure chooses many M dwarfs.
- For a given effective temperature, the stars for which planets are detected in the full frame images are systematically fainter, compared to PS stars. Projecting the FFI detections onto apparent I_c

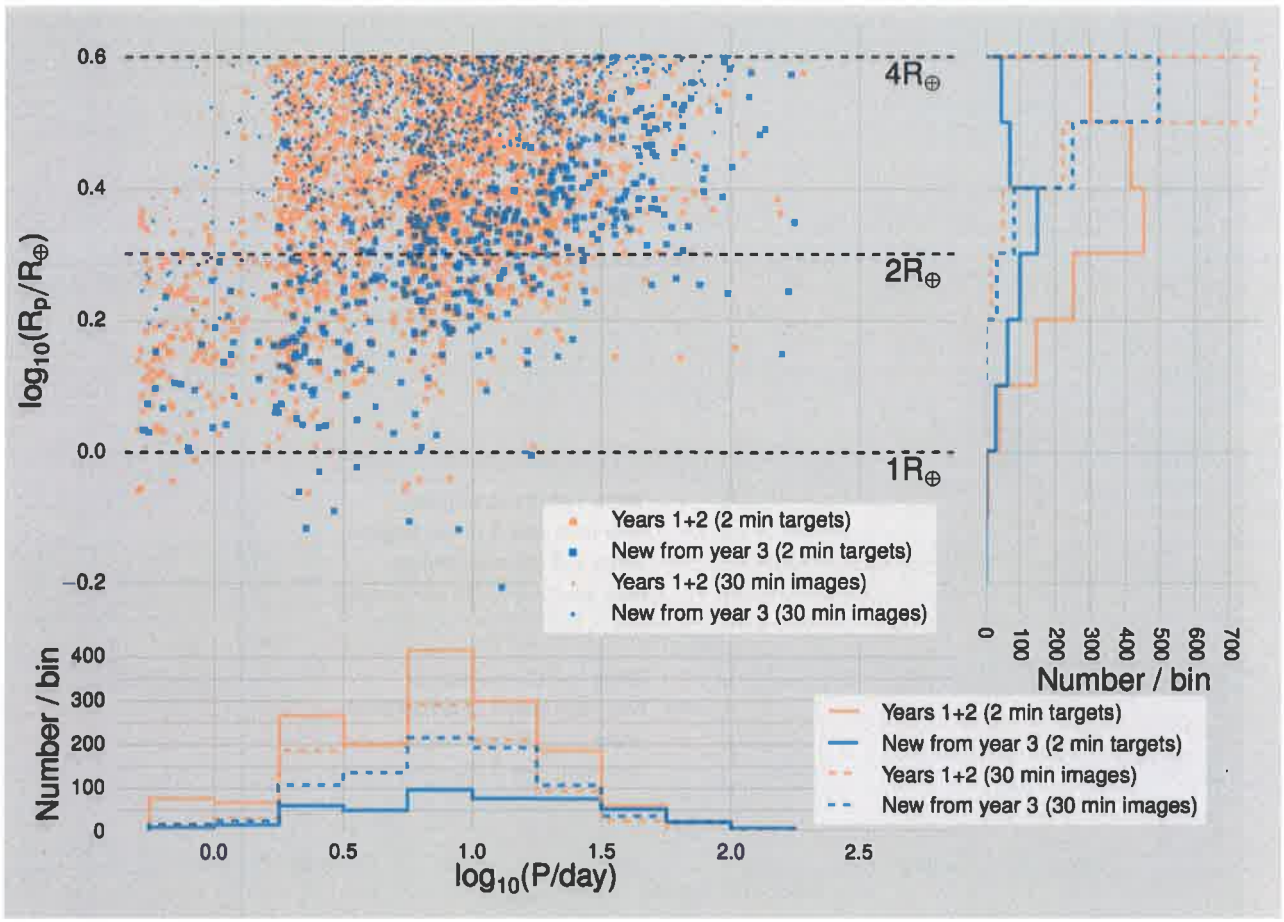

Figure 12: Radius vs period of detected $R_p < 4R_\oplus$ planets from one Monte Carlo realization of the `hemi` scenario. At a fixed period, Extended Missions help us detect smaller planets; at a fixed radius, they let us probe out to longer periods. The radius histogram, and the location of all dots (rather than squares) on the scatter plot show that almost all $R_p < 2R_\oplus$ planets are detected in postage stamps, not full frame images (also shown in Fig. 10).

magnitude (Fig. 13, right panel), the median brightness of stars with planets detected from FFIs is actually greater than the median brightness of planets detected from PSs. This is because the FFI-based detections involve stars with radii that, on average, are greater than those from postage-stamp detections.

There are a few other statistics that interesting for purposes of characterizing the value of this Extended Mission – how many new planets do we detect? How many are at long orbital periods? How many are in habitable zones? We respond to these questions in Sec. 2.3, in particular showing our detected planet yields in Fig. 14.

2.3 *Comparing planet yields from all Extended Missions based on new planet detection metrics*

To compare Extended Missions in terms of planet detection statistics, we focus on the subset of all detected planets that are *newly* detected

are

is it also because of the selection procedure (add in enough M dwarfs and you can pull the PS distribution to very faint stars)

redundant to the clearer bulletized stuff in §2.3.

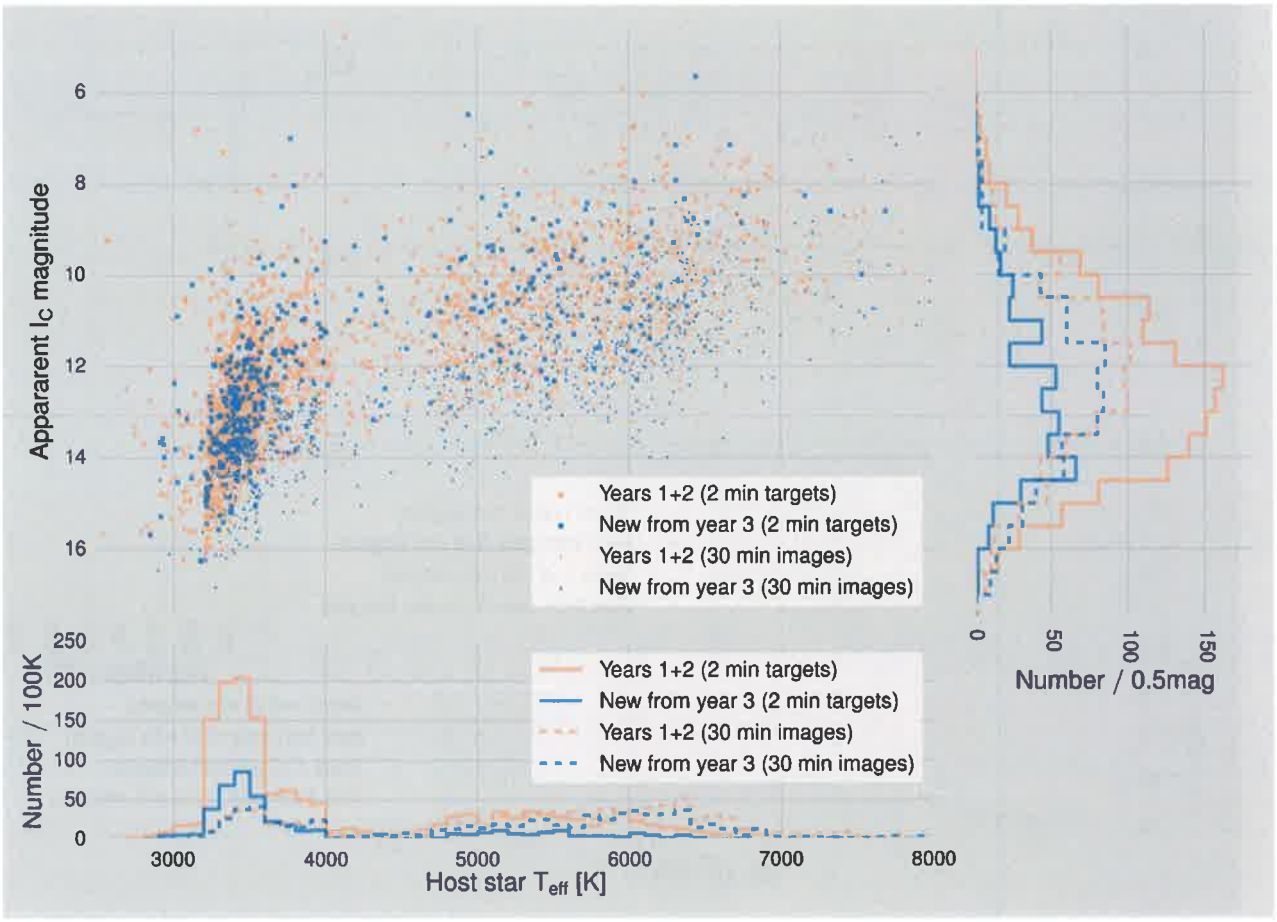

Figure 13: Apparent Cousins I magnitude plotted against effective temperature for $R_p < 4R_\oplus$ planets detected from one Monte Carlo realization of the `hemi` scenario. Postage stamp (PS) detections are biased towards M dwarfs in part because of our selection procedure. For a given effective temperature, full frame images (FFIs) are taken of dimmer stars.

from each Extended Mission. These may come from stars that were not observed at all in the Primary Mission (notably for scenarios such as `ecl_long`), or they may also come from transiting planets that were observed in the Primary Mission with SNR < 7.3, or from planets that were single-transiters in the Primary Mission (we require $N_{\rm tra} \geq 2$) for detection. With this in mind, for each Extended Mission scenario we ask the following questions:

1. $N_{\rm new}$: How many new planets do we detect?
2. $N_{\rm new,P>20d}$: How many of these new planets are at long orbital periods, for instance $P > 20$ days?
3. $N_{\rm new,HZ}$: How many are in the habitable zone?
4. $N_{\rm sys,extra\ planets}$: In how many systems in which at least one planet was detected during the Primary Mission do we find extra planets in the Extended Mission?

pages 31 ff

not included

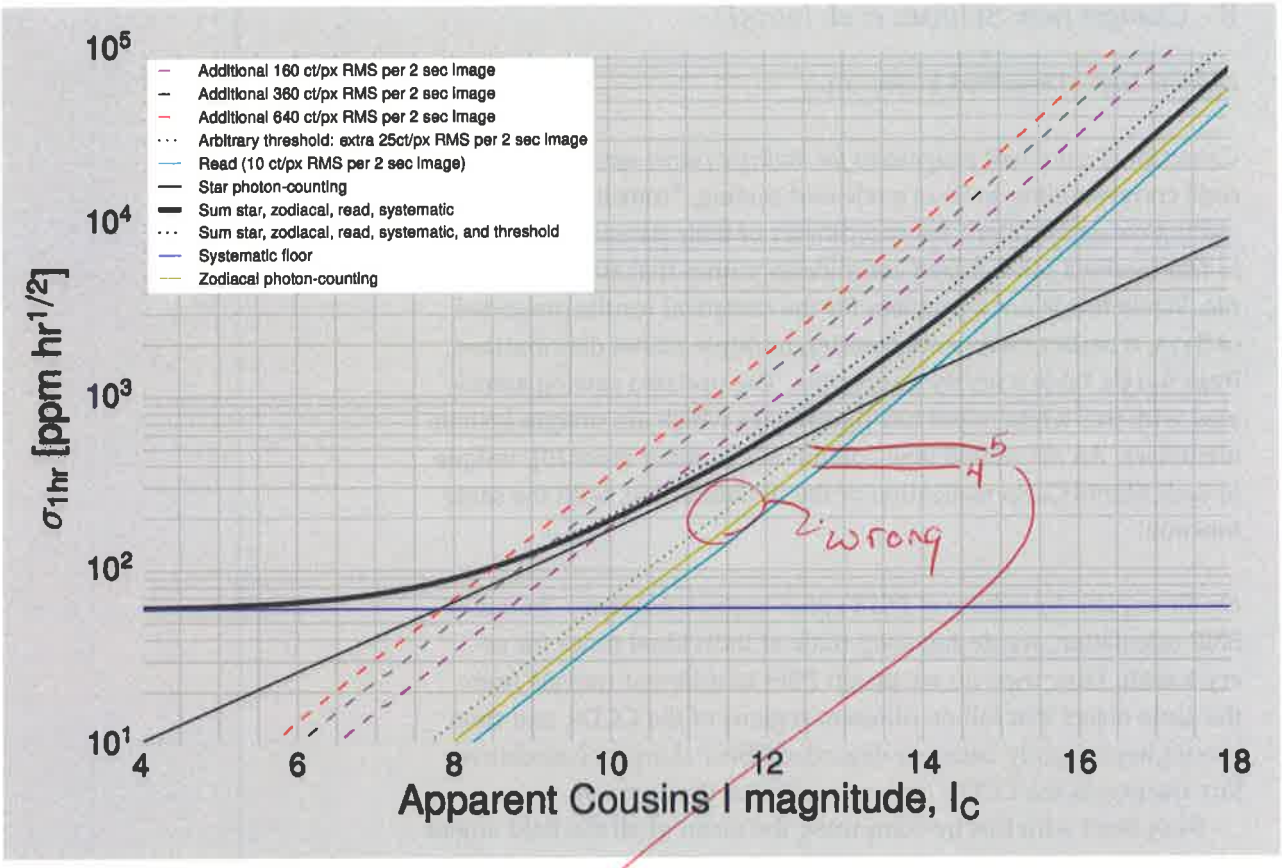

Figure 27: Same as Fig. 7, with threshold $F_{\rm thresh}$ of Sec. 1.6 overplotted (dotted green line). The expected noise budget is the thick black line; adding the threshold to it yields the dotted black line. As indicated in the text, this particular threshold is defined so that it is sensitive to even slight reductions in photometric sensitivity at $I_c \lesssim 13$.

See p. 21, the dotted line corresponding to 300 ct/px/s should be 2x higher than the "Zodi photon-counting" line, but you've under estimated the effect as $\sim \frac{5}{4} = 1.25$ instead of 2.0.

B *Changes from Sullivan et al. [2015]*

Dilution bug. Described in Sec. 2.1.

Correction of coordinate assignment for multiple planet systems. In the code corresponding to S+15's released catalog, "transiting objects" did not correctly inherit the coordinates of their parent star – they in fact received randomized coordinates within that star's HealPix tile. While this is not a problem for the statistical results presented in S+15, it makes reverse-engineering multiple planet distributions from S+15's Table 6 nearly impossible. The updated catalog associated with this white paper has coordinates which are unique system identifiers. An associated new column is a number (`hostID`), unique to each Monte Carlo realization of the updated code, with the same function.

On the angular dependence of TESS's pixel response function: In our SNR calculation, we do not keep track of individual times for every transit. How then do we assign PSFs to different transits from the same object that fall on different regions of the CCDs, and thus should have slightly better or degraded PSFs? (Largest cumulative flux fraction at the CCD's center, smallest at the corners).

S+15 dealt with this by computing the mean of all the field angles (distance from the center of the CCD axis), and then passing this mean into a look-up table for PSFs based on four PSFs that had been computed from a ray-tracing model at four different field angles. S+15 then 'observes' each eclipsing object with a single class of PSF. This leads to the implausible phenomenon that extra observations can actually *lower* the SNR of an eclipsing object if they are taken with an unfavorable field angle/PSF. This effect is largely off-set by the extra pointing increasing the SNR, but for Extended Missions (coming back to the same objects at potentially very different field angles) it winds up reducing observed SNR for $\sim$3% of detected objects.

In Extended Missions (as well as in the Primary Mission) we expect stars to land on very different regions of the CCD over the course of being observed. We simplify this in our work by assuming that all stars land on the center of the *TESS* CCDs (the green curve of S+15 Fig. 13). This assumption is justified because our chief point of quantitative comparison is the ability of different pointing strategies to impact *TESS*'s planet yield in Extended Missions, and there is little *a priori* reason to assume that any one pointing scenario should be biased for an extra amount of stars to land on the 'bad regions' of *TESS*'s CCDs.